

Physics Constrained Flow Neural Network for Short-Timescale Predictions in Data Communications Networks

Xiangle Cheng,¹ James He,² Shihan Xiao,^{1*} Yingxue Zhang,³ Zhitang Chen,⁴ Pascal Poupart,² Fenglin Li¹

¹ Huawei 2012 Network Technology Lab

² University of Waterloo

³ Huawei Technologies Canada

⁴ Huawei Noahs Ark Lab

{chengxiangle1, xiaoshihan, yingxue.zhang, chenzhitang2, lifenglin}@huawei.com, {james.he, ppoupart}@uwaterloo.ca

Abstract

Machine learning is gaining growing momentum in various recent models for the dynamic analysis of information flows in data communications networks. These preliminary models often rely on off-the-shelf learning models to predict from historical statistics while disregarding the physics governing the generating behaviors of these flows. This paper instead introduces **Flow Neural Network (FlowNN)** to improve the feature representation with learned physical bias. This is implemented by an induction layer, working upon the embedding layer, to impose the physics connected data correlations, and a self-supervised learning strategy with stop-gradient to make the learned physics universal. For the short-timescale network prediction tasks, FlowNN achieves 17% ~ 71% of loss decrease than the state-of-the-art baselines on both synthetic and real-world networking datasets, which shows the strength of this new approach. Code will be made available.

Keywords: Flow Neural Network, Physical Bias, Stop-gradient, Flow Prediction

Introduction

Data communications networks provide the majority of data transmission services to support today’s Internet applications and have huge social values. This paper is concerned with a dynamic analysis model dealing with flows of information with sources and destinations in a data communications network. As depicted in Fig. 1, the source of a flow is a node (computer, phone, router/ switch etc.) in the network from which packets¹ start their travels and the destination is where they end. Throughout the lifespan of a flow (e.g., a 10-minute phone call or a 2-hour online video), packets consistently traverse along the assigned routing path connecting the source and destination. Depending on the real-time congestion conditions of nodes on the routing path, packets may experience different buffering or retransmission delays, resulting in varying transmission rate and service delay.

A good understanding of the behavioral patterns of the underlying packets and flows plays a crucial role in network planning, traffic management, as well as optimizing Quality

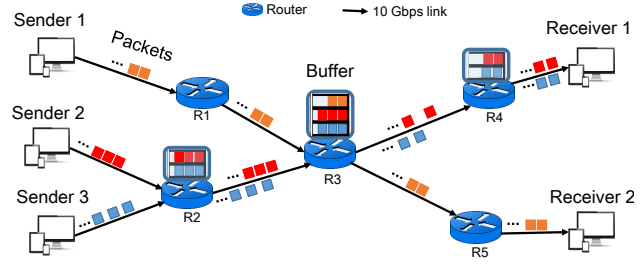


Figure 1: Packet flows in data communications networks.

of Service (QoS, e.g., transmission rate, delay, etc.). However, the high nonlinearity and dynamics of the networking system often make it difficult to make fine-grained analysis. Consider the illustrative example in Fig. 2, which plots the traffic rate traces we collected from a real-world network–*WIDE*². This shows the *realistic* traffic patterns when the real-time data transmission rate is averaged by two different time scales. The longer-timescale plot in Fig. 2b shows a clear periodicity associated with daily human activities. By contrast, the traffic trace in Fig. 2a gets more noisy and difficult to recognize obvious patterns when they are averaged every millisecond.

Therefore, recent works often rely on off-the-shelf machine learning models to predict from the data statistics of a flow. The remarkable advances, as achieved in long-timescale prediction tasks (e.g., at seconds or minutes intervals (Marcus et al. 2020; Mozo, Ordozgoiti, and Gómez-Canaval 2018)), are a testament to this minimalist principle. A key limitation of these machine learning models is that they disregard the physics governing the generating behaviors of these packet flows.

In practice, the dynamics of spatio-temporal flow evolutions are governed by physical laws or models operating the networking system. For instance, in networks with TCP/IP protocol suite, the real-time transmission rates of different packet sources are typically modulated dynamically by congestion control models to prevent congestive collapse (Nathan et al. 2019); The conservation law describes the macroscopic fluid dynamics of data flows during hop-by-

*Corresponding author.

¹Information is encoded in packets, which can be seen as particles travelling in the network.

²Data is publicly available at <https://mawi.wide.ad.jp/mawi/>

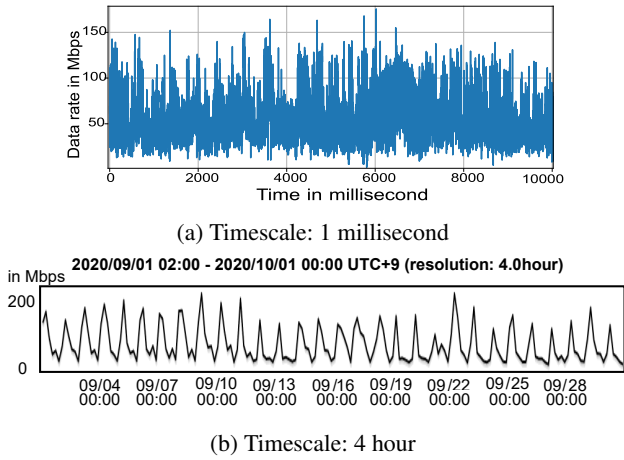


Figure 2: Time series of real-world traffic rate traces from WIDE network binned by two different time scales.

hop transmissions (Apice, Manzo, and Piccoli 2008). The physics establishes the *inductive bias* (Peter et al. 2018) when predicting from history. That is, the future is not entirely random or *noisy* even when observed at a millisecond granularity, but can be connected from physical models or laws with its history.

In this paper, we investigate how to represent such essential physical bias in a learning model to improve the short-timescale flow predictions. Accordingly, we propose **Flow Neural Network (FlowNN)**, the first customized learning model for the data analysis of networking flows, with full respect for the packet routing structure and working mechanism.

Our contributions can be summarized as follows: (1) We develop FlowNN, a learning model, to exploit at the first time the physical data correlations connected by the congestion control model and flow conservation law in data communications networks; (2) We design a self-supervised learning strategy with stop-gradient, which can learn the feature representation and physical bias simultaneously at each gradient update step; (3). We show with realistic packet datasets that FlowNN achieves the state-of-the-art results and outperforms the incumbent baselines by 17% ~ 71% of loss decrease for the short-timescale prediction problems.

Preliminaries

Packet Flow. A s - d flow is a sequence of packets encapsulating the message bits and get forwarded from source s along an assigned routing path $P \in \mathbb{Z}^L$ to destination d . Let $x_{f,n}^t \in \mathbb{R}$ be the value of feature f measured at node $n \in P$ during the time interval t . For instance, $x_{f,n}^t$ can be the average packet travelling delay or transmission/receiving rate of a flow. Let us denote the time-series tensor of a flow as $X^t = \{x_n^t\}_{n=1, \dots, L} \in \mathbb{R}^{L \times N_f}$. With telemetry monitors installed at each node, we can collect the running traces of X^t as Fig. 3a.

Packet Flow Prediction Problem. Given the time-series tensor X^t of a flow in the form of Fig. 3a, predict its future

Table 1: key symbol notations

L, N_f, d, N	length of a routing path P , number of features, number of hidden dimensions and number of recurrent iterations in FlowNN, respectively
$x_{f,n}^t \in \mathbb{R}$	value of feature f at node $n \in P$, and $x_{r,n}^t$ specifically denotes the transmit/receive rates
$x_n^t \in \mathbb{R}^{N_f}$	a set including all N_f features at n and t
$X^t \in \mathbb{R}^{L \times N_f}$	time-series tensor of a flow at t
$\hat{h}_n^t \in \mathbb{R}^d$	hidden vector of node n at t
f_{L_1}	neural net for initial embedding of x_n^t
f_{L_2}	compound neural net with a multi-layer perceptron (MLP) and a recurrent net to aggregate all \hat{h}_n^t along dimension- n and then dimension- t
f_{L_3}	compound neural net with a MLP net f_S to aggregate the states of two neighboring nodes at aligned t , and a Seq2Seq net to predict the target window from its correlated source window

service qualities, such as next-step service delay or transmission/receiving rate.

Congestion Control. A congestion control model can be regarded as mapping a locally-perceived history of feedback from the receiver, which reflects past traffic and network conditions, to the next choice of sending rate (Nathan et al. 2019). Such built-in controls in today’s networking systems can avoid congestive collapse resulting from oversubscription (refer to Appendix for more details). Such physical models, along with the following conservation law, can be harvested to refine the output space of a prediction as *soft* constraints.

Flow Conservation Law. For a packet flow, assume r_{uv}^t is the bit rate that a flow receives at node $v \in P$ from node $u \in P$ at time t . Then, we have the following conservation constraint³:

$$\sum_t r_{uv}^t = \sum_t r_{v,w}^t = b_v, \forall (u, v, w) \subseteq P \quad (1)$$

where b_v are the cumulative amount of flow bits the source sends out.

Eq. 1 analytically constrains the bit rates sent and received at each node along the routing path. The cumulative amount of forwarded flow bits are conserved among the routing nodes. Consequently, the rates between two neighboring routing nodes will become larger and smaller by turn during the flow lifespan. As shown in Fig. 3b, this explicitly forms a set of correlated time windows. During source window T_1 , a node has a larger (or smaller) rates than its successor node. Then, a target window T_2 is always followed, in which the node will have a smaller (or larger) rates than its predecessor node. Such property is resulted from the routing structure and packet buffering mechanism in communi-

³Packets may be lost with a probability when congestion occurs and each lost packet will be sent again. With congestion models and buffering mechanisms, the loss probability is quite small ($< 0.1\%$) in current commercial networking systems.

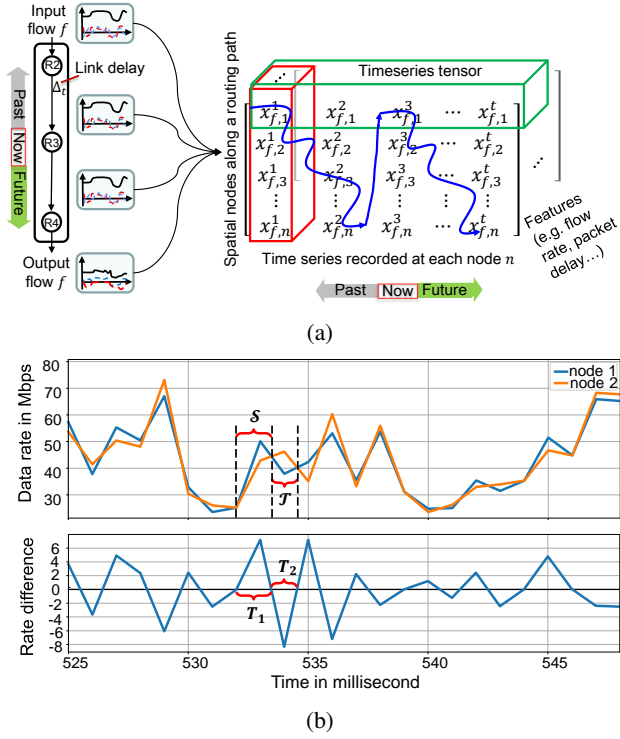


Figure 3: (a) Data of a packet flow in the form of time-series tensor. The blue curve characterizes the data correlation-propagated along the spatio-temporal dimensions; (b) A sample of data rates of a flow and the observed rate difference between two neighboring routing nodes. The sequences \mathcal{S} in source time window T_1 are highly correlated with the sequences \mathcal{T} in target time window T_2 by the effect of flow conservation.

cations networks, and is independent of network and flow configurations.

Accurately modelling of the flow dynamics requires attention to above domain-specific physics and properties, which are absent in the majority of existing learning models if not all of them.

Next, we introduce FlowNN to represent these physics as learning bias to improve the data analysis. Fig. 4 abstracts the architectural differences among different models.

Remark 1: We are not resorting to learning a strict conservation constraint with FlowNN. Alternatively, we introduce the resulted correlation window as a *soft constraint* or *relational inductive bias* (Peter et al. 2018) to directly estimate each state \hat{h}_n^t from its most related data.

Flow Neural Network

Our architecture (Fig. 5) consists of three learnable neural network functions, denoted as f_{L_1} , f_{L_2} , f_{L_3} , respectively. FlowNN works upon the initial embedding/encoding layer L_1 to further impose the physics connected learning bias.

Concretely, for the time-series tensor of each flow $X^t = \{x_n^t\}_{n=1, \dots, L} \in \mathbb{R}^{L \times N_f}$, f_{L_1} first projects each $x_n^t \in \mathbb{R}^{N_f}$

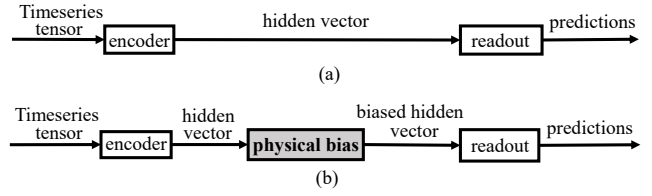


Figure 4: Comparison on different learning architectures: (a) existing learning models; (b) FlowNN.

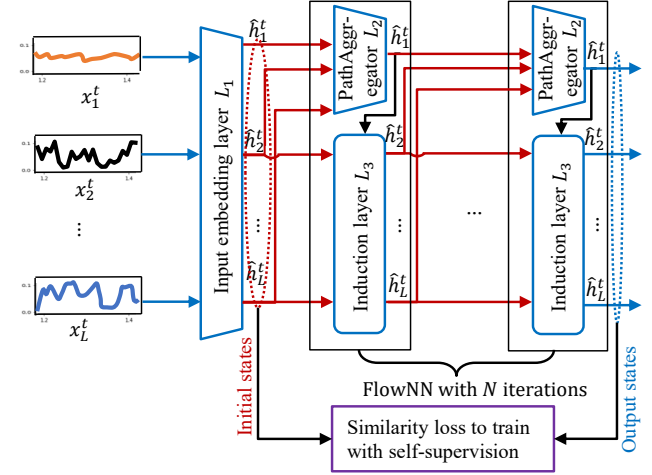


Figure 5: FlowNN architecture.

to latent space \mathbb{R}^d :

$$\hat{h}_n^\tau = f_{L_1}(x_n^\tau), \forall \tau = t_0, \dots, t-1; n = 1, \dots, L \quad (2)$$

Then, PathAggregator f_{L_2} uses a MLP to aggregate $\hat{H}^\tau = \{\hat{h}_n^\tau\}_{\tau=t_0, \dots, t-1; n=1, \dots, L}$ from layer L_1 along dimension- n and a recurrent net (e.g., GRU) to aggregate over $\tau = t_0, \dots, t-1$:

$$\hat{h}_1^t = f_{L_2}(\hat{H}^\tau) = GRU(MLP(\{\hat{h}_n^\tau\}_{n=1, \dots, L})) \quad (3)$$

The PathAggregator aggregates the locally-perceived traffic and network conditions along the routing path, which can be mapped to its next sending rate from the source. It physically plays the role of a simulator to imitate the decision process of existing congestion control models.

With the aggregated state \hat{h}_1^t and initial hidden states $\{\hat{h}_n^t\}_{n=2, \dots, L}$, the Induction layer L_3 is then applied to further learn the biased relations between source time windows and target time windows. Specifically, for each pair⁴ of two neighboring nodes $\langle n, n+1 \rangle$, $n = 0, \dots, L-1$, we split the associated time-series \hat{h}_n^τ into a set of correlation windows $\langle T_1^i, T_2^i \rangle_{i=1, 2, \dots}$ according to the time-series delta $x_{r,n}^\tau - x_{r,n+1}^\tau$ of the transmission rates between the two neighboring nodes (as shown in Fig. 3b and Algorithm 1). For each correlated window $\langle T_1^i, T_2^i \rangle$, we encode the hid-

⁴ $\langle \cdot \rangle$ denotes the paired set of the two included elements.

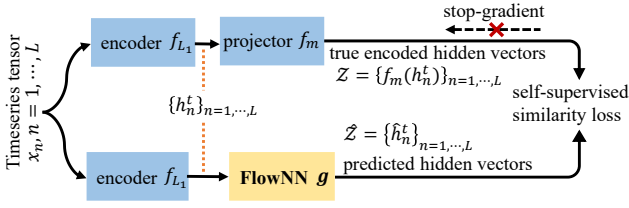


Figure 6: Self-supervised FlowNN training architecture.

den states of sequences in T_1^i and T_2^i as follows:

$$\hat{h}_{n+1}^\tau = f_S(\{\hat{h}_1^{\tau-1} \parallel h_{n+1}^{\tau-1}\}), \forall \tau \in T_1^i \quad (4)$$

$$\{\hat{h}_{n+1}^\tau\}_{\tau \in T_2^i} = f_T(\{h_{n+1}^{\tau-1}\}_{\tau \in T_2^i} \mid \{\hat{h}_1^\tau\}_{\tau \in T_1^i}) \quad (5)$$

where f_S is a MLP, and f_T is a sequence to sequence (Seq2Seq) net (Sutskever, Vinyals, and Le 2014) to predict $\{\hat{h}_{n+1}^\tau\}_{\tau \in T_2^i}$ conditioned on the states of $\{\hat{h}_1^\tau\}_{\tau \in T_1^i}$. Here, \parallel and \mid are concatenation and conditional operators, respectively.

Eq. 4 introduces path-level messages into the locally-perceived states and then propagates the state messages to the next time step of $n+1$. Eq. 5 predicts the states of sequences in T_2^i at $n+1$ conditioned on the states of history window T_1^i .

The steps from Eq. 3–5 explicitly represent the natural data connections in Fig. 3a, resulted from the congestion control and hop-by-hop packet transmission. As shown in Fig. 5, the predicted outputs $\{\hat{h}_n^t\}_{n=1, \dots, L}$ can be recurrently input into the same PathAggregator L_2 and Induction layer L_3 to propagate messages by the rules of Eq. 3–5 to farther distance along spatio-temporal dimensions. The number of recurrent iteration N is a tunable hyperparameter.

Self-Supervised Training Strategy

The self-supervised FlowNN training architecture (Fig. 6) has two processing branches, working on a shared initial embedding layer (encoder) f_{L_1} . The bottom branch uses FlowNN to impose physical learning bias to predict on the hidden states from f_{L_1} . The top branch uses a linear projection f_m to transform the output from f_{L_1} into another view. Denote the output vectors of the two branches as $Z = \{f_m(h_n^t)\}_{n=1, \dots, L}$ and $\hat{Z} = \{\hat{h}_n^t\}_{n=1, \dots, L}$. Similar to (Grill et al. 2020; Chen and He 2021), we define the following symmetrized loss to minimize their negative cosine similarity:

$$\mathcal{L} = -\frac{\cos(\hat{Z}, \text{stopgrad}(Z))}{2} - \frac{\cos(\text{stopgrad}(\hat{Z}), Z)}{2} \quad (6)$$

where $\text{stopgrad}(Z)$ operation detaches Z from the gradient computation, and thus encoder f_{L_1} receives no gradient from Z (and vice versa for \hat{Z}).

The training strategy in Fig. 6 is inspired by both SimSiam and Contrastive Predictive Coding (CPC) (Oord, Li, and Vinyals 2019). But we combined their advances and extended their applications to the concerned prediction tasks, rather than a standard application.

Algorithm 1: FlowNN pseudocode

Input: $\{x_n^\tau\}_{\tau=t_0, \dots, t-1, n=1, \dots, L}$ # note: $x_{r,n}^\tau \in x_n^\tau$

Output: $\{\hat{h}_n^\tau\}_{\tau=t, n=1, \dots, L}$ # predicted representation

- 1: $\hat{h}_n^\tau = f_{L_1}(x_n^\tau), \forall \tau = t_0, \dots, t-1; n = 1, \dots, L$
- 2: **for** all N recurrent iterations **do**
- 3: #PathAggregator
- 4: $\hat{h}_1^\tau = f_{L_2}(\{\hat{h}_n^\tau\}_{n=1, \dots, L}), \forall \tau = t_0, \dots, t-1$
- 5: **for** all neighboring pairs $\langle n, n+1 \rangle_{n=1, \dots, L-1}$ **do**
- 6: $\langle T_1^i, T_2^i \rangle_{i=1, 2, \dots} = \text{split}(\{x_{r,n}^\tau - x_{r,n+1}^\tau\}_{\tau=t_0, \dots, t-1})$
- 7: $\{\hat{h}_{n+1}^\tau\}_{\tau=t_1, \dots, t} = \text{Induction}(\langle T_1^i, T_2^i \rangle_{i=1, 2, \dots}, \{\hat{h}_1^\tau, h_{n+1}^\tau\}_{\tau=t_0, \dots, t-1})$
- 8: **end for**
- 9: **end for**

Def split()

- Input:** $\{x_{r,n}^\tau - x_{r,n+1}^\tau\}_{\tau=t_0, \dots, t-1}$
- 1: set correlation window index $i = 0, T_1^i = T_2^i = []$
 - 2: **for** all $\tau = t_0, \dots, t-1$ **do**
 - 3: **if** $x_{r,n}^\tau - x_{r,n+1}^\tau \geq 0$ **then**
 - 4: append τ to T_1^i
 - 5: **end if**
 - 6: **if** $x_{r,n}^\tau - x_{r,n+1}^\tau < 0$ **then**
 - 7: append τ to T_2^i
 - 8: **end if**
 - 9: **if** $x_{r,n}^\tau - x_{r,n+1}^\tau < 0$ and $x_{r,n}^\tau - x_{r,n+1}^\tau \geq 0$ **then**
 - 10: $i = i + 1, T_1^i = T_2^i = []$
 - 11: **end if**
 - 12: **end for**
 - 13: **return** $\langle T_1^i, T_2^i \rangle_{i=1, 2, \dots}$

Def Induction()

- Input:** $\langle T_1^i, T_2^i \rangle_{i=1, 2, \dots}, \{\hat{h}_1^\tau, h_{n+1}^\tau\}_{\tau=t_0, \dots, t-1}$
- 1: $\hat{h}_n^t = f_p(\hat{h}_1^t), \forall t \in \{T_1^i, T_2^i\}$
 - 2: **for** each $i = 1, 2, \dots$ **do**
 - 3: $\hat{h}_{n+1}^t = f_S(\{\hat{h}_n^{t-1} \parallel h_{n+1}^{t-1}\}), \forall t \in T_1^i$
 - 4: $\{\hat{h}_{n+1}^t\}_{t \in T_2^i} = f_T(\{h_{n+1}^{t-1}\}_{t \in T_2^i} \mid \{\hat{h}_n^\tau\}_{\tau \in T_1^i})$
 - 5: **end for**
 - 6: **return** $\{\hat{h}_{n+1}^\tau\}_{\tau=t_1, \dots, t}$

Concretely, CPC demonstrates that predicting the future improves the representation in latent space. But CPC still relies on large batches and negative samples to train a contrastive loss. Xinlei and Kaiming reported in SimSiam the surprising results achieved without negative sample pairs and large batches. Inspired by both, we found the strategies of SimSiam can also be applied to augment the training of the regression model in CPC. As annotated in Fig. 6, the output of the bottom pipeline is the predicted hidden vectors (the information at t is NOT included when predicting for time t with FlowNN). If we first remove the component of f_m , the upper pipeline produces the true encoded hidden vectors from f_{L_1} with the information at t included (thus this can be treated as the ground truth of hidden vectors in latent space). The loss here is constructed to make the predicted hidden vectors agree with the true encoded hidden vectors.

The pretraining process tries to learn with FlowNN the physical bias resulted by the built-in system working mechanism of networks. With f_m , FlowNN will be trained to respect the approximated expectation of all possible input (similar to the predictor h in SimSiam). This makes the learned physical bias from FlowNN stable across different input. This precisely explains the good transferability of the pretrained FlowNN in Out-Of-Distribution test (Table 4) and cross-task test (i.e., delay prediction in Table 3). See (Chen and He 2021) and Appendix for more explanations. Algorithm 1 describes the overall pseudocodes of FlowNN.

Remark 2: In experiments for Algorithm 1, f_{L_2} used GRU-type recurrent net. $f_{\mathcal{T}}$ is a Seq2Seq net implemented by two separate GRUs to encode and decode the source and target sequences, respectively, although FlowNN is not limited to the chosen GRU models. More advanced models (e.g., latest attention mechanisms) can be also exploited for further improvement.

Remark 3: For FlowNN, the computation complexity is $\mathcal{O}(L)$, depending on the length of routing paths rather than the size of the whole graph. To fit variant-length routing path, mechanisms to tackle the input and output sequences with variant lengths in natural language processing (NLP) tasks also work for FlowNN, such as padding and masking, or using Seq2Seq net as encoder.

Experiments

We empirically perform experiments to predict the end-to-end packet transmission delay and transmission/receiving rates r_{uv}^t along the routing path of each flow, which are closely connected with the packet flow patterns.

Datasets. Four publicly available datasets—*WIDE*, *NUMFabric*⁵, *NSF* and *GM50*⁶ are used. *WIDE* are the realistic traffic traces collected from real-world network environment (WIDE 2020), and the others are the synthetic traffic widely applied in recent networking researches (Nagaraj et al. 2016; Lei et al. 2019). We sampled 50 flows at the timescale of $1ms$ for total length $30000ms$. The included raw features in the time-series tensor of each flow are the transmission rates (or receiving rates at destinations), as well as the associated aggregated rates at each routing node. Each flow has a routing path with 5 nodes in *WIDE* and *NUMFabric*, and variant-length routing paths ranging from 2 to 7 in *NSF* and *GM50*. In all experiments, we split the first 40 flows to train, validate and test by ratio 6:2:2, and the remaining 10 flows are retained to test the performance of the model on unseen flows after training.

Baselines. We have compared FlowNN with the following most related baselines: 1) Auto-Regression Integrated Moving Average (ARIMA) (Wang, Smith-Miles, and Hyndman 2006); 2) GRU (Chung et al. 2014); 3) multivariate GRU (m-GRU); 4) STHGCN (Marcus et al. 2020), and 5)

⁵The data can be generated by running the simulation code released in <https://bitbucket.org/knagaraj/numfabric/src/master/>.

⁶*NSF* and *GM50* are synthetic datasets from <http://www.knowledgedefinednetworking.org/>.

STGCN (Yu, Yin, and Zhu 2018). Particularly, GRU encodes and predicts each time-series sequence independently without any reference to the information from other spatial nodes. In contrast, m-GRU processes joint information from all routing nodes to predict. STHGCN is the very recent work for networking traffic analysis, which uses graph convolutional network (Kipf and Welling 2016) and GRU to predict the spatial states of all nodes at each time. Finally, STGCN is a widely used model for transportation traffic analysis, which is built upon the spatio-temporal graph convolution net. The compared baselines treat the time-series tensor of a flow as multivariate input (GRU, m-GRU) or graph-type input (STHGCN, STGCN), which are the dominant approaches to model spatio-temporal relationships in the existing studies. We conduct grid search over the hyperparameters for all baselines. The recurrent iteration $N = 2$ is chosen. The details of model configurations and hyperparameter search procedure are given in Appendix. Experiments are conducted on a single Nvidia P40 24GB GPU.

Evaluation metrics. We used the following metrics to evaluate the prediction quality of \hat{y} with the ground truth y .

$$\text{Mean squared error: } MSE = \frac{1}{n} \sum_{i=1}^n (y_i - \hat{y}_i)^2 \quad (7)$$

$$\text{Relative squared error: } RSE = \frac{\sum_{i=1}^n (y_i - \hat{y}_i)^2}{\sum_{i=1}^n (y_i - \bar{y})^2} \quad (8)$$

Correlation coefficient:

$$Corr = \frac{\sum_{i=1}^n (y_i - \bar{y})(\hat{y}_i - \hat{\bar{y}})}{\sqrt{\sum_{i=1}^n (y_i - \bar{y})^2} \sqrt{\sum_{i=1}^n (\hat{y}_i - \hat{\bar{y}})^2}} \quad (9)$$

where \bar{y} and $\hat{\bar{y}}$ are the mean values of y and \hat{y} .

Linear evaluation on rate prediction task. We first evaluate the learned latent representation $\{h_n^t\}_{n=1, \dots, L}$ of FlowNN for the rate prediction task by finetuning a MLP readout layer on top of the pretrained FlowNN model. During the finetuning process, the pretrained FlowNN model is further optimized according to ground-truth labels. By contrast, the compared baselines are directly trained together with their MLP readout layers.

Table 2 reports the test performance of next-step ($1ms$) predictions. Here, *Naive* approach directly takes the current value as next-step prediction. The results of *Naive* and ARIMA provide evidents that the traditional statistic time-series prediction models fail to provide reasonable performance on short-timescale prediction tasks. We can observe that FlowNN outperforms all baselines, achieving a MSE decrease of up to 71% (GRU), 17% (m-GRU), 36.8% (STHGCN), and 44.4% (STGCN).

Fig. 7 shows the test performances of different models on multi-step-ahead prediction task. Following the practice of second-granularity traffic forecasting in (Mozo, Ordozgoiti, and GoÁmez-Canaval 2018), we target at predicting the average values across next multiple steps. That is, we predict the value of $\mathbb{E}[x^{t+1}, \dots, x^{t+\Delta}]$, where Δ is the time length

Table 2: Test performance comparisons

Dataset Model		Test on seen flows			Test on unseen flows		
		MSE	RSE	Corr	MSE	RSE	Corr
NUMFabric	Naive	0.3567	0.6175	0.8091	-	-	-
	ARIMA	0.2724	0.5199	0.8543	-	-	-
	GRU	0.0872±0.0013	0.3021±0.0018	0.9533±0.0006	0.0895±0.0033	0.3092±0.0038	0.9510±0.0013
	m-GRU	0.0306±0.0004	0.1789±0.0013	0.9840±0.0002	0.0311±0.0010	0.1823±0.0025	0.9833±0.0005
	STHGCN	0.0405±0.0006	0.2060±0.0013	0.9785±0.0003	0.0417±0.0014	0.2109±0.0026	0.9775±0.0006
	STGCN	0.0457±0.0007	0.2186±0.0018	0.9758±0.0006	0.0453±0.0012	0.2200±0.0039	0.9755±0.0018
	FlowNN	0.0254±0.0003	0.1632±0.0010	0.9867±0.0002	0.0261±0.0009	0.1672±0.0021	0.9860±0.0004
WIDE	Naive	0.8384	0.9420	0.5533	-	-	-
	ARIMA	0.4879	0.6422	0.7668	-	-	-
	GRU	0.5857±0.0074	0.7764±0.0057	0.6325±0.0071	0.5508±0.0113	0.7539±0.0088	0.6585±0.0103
	m-GRU	0.4609±0.0061	0.6887±0.0059	0.7271±0.0055	0.4490±0.0087	0.6807±0.0086	0.7345±0.0080
	STHGCN	0.4878±0.0063	0.7085±0.0056	0.7079±0.0055	0.4710±0.0096	0.6971±0.0084	0.7191±0.0084
	STGCN	0.4967±0.0021	0.7151±0.0013	0.7073±0.0014	0.4695±0.0048	0.6961±0.0032	0.7258±0.0034
	FlowNN	0.4123±0.0054	0.6514±0.0058	0.7599±0.0050	0.4007±0.0078	0.6430±0.0085	0.7674±0.0073
NSF	Naive	0.2244	0.5006	0.8742	-	-	-
	ARIMA	0.2240	0.4852	0.8745	-	-	-
	GRU	0.1168±0.0030	0.3576±0.0046	0.9341±0.0018	0.1140±0.0047	0.3814±0.0052	0.9253±0.0021
	m-GRU	0.0794±0.0022	0.2948±0.0041	0.9556±0.0013	0.0888±0.0040	0.3366±0.0050	0.9423±0.0018
	STHGCN	0.0938±0.0024	0.3204±0.0042	0.9474±0.0014	0.1302±0.0065	0.4075±0.0071	0.9157±0.0028
	STGCN	0.1214±0.0016	0.3643±0.0027	0.9333±0.0013	0.1222±0.0034	0.3944±0.0055	0.9213±0.0035
	FlowNN	0.0791±0.0021	0.2942±0.0039	0.9558±0.0012	0.0851±0.0035	0.3296±0.0043	0.9446±0.0015
GMS0	Naive	1.3387	1.1929	0.2806	-	-	-
	ARIMA	0.5383	0.7687	0.6410	-	-	-
	GRU	0.6381±0.0151	0.8179±0.0113	0.5756±0.0164	0.8921±0.0116	0.9494±0.0064	0.3148±0.0274
	m-GRU	0.5628±0.0143	0.7682±0.0116	0.6405±0.0134	0.8168±0.0110	0.9084±0.0064	0.4184±0.0147
	STHGCN	0.5853±0.0149	0.7834±0.0117	0.6218±0.0143	0.8427±0.0123	0.9227±0.0076	0.3866±0.0175
	STGCN	0.5877±0.0021	0.7850±0.0017	0.6206±0.0023	0.8329±0.0051	0.9175±0.0020	0.3997±0.0040
	FlowNN	0.5429±0.0138	0.7544±0.0114	0.6567±0.0125	0.7958±0.0106	0.8967±0.0061	0.4431±0.0131

to predict. This information is crucial to many short-term networking planning and control tasks in communications networks. In this task, FlowNN are consistently best for different time steps ahead predictions. Note that for any $\Delta \geq 2$, it is not always harder or easier to predict under the different degree of traffic burstiness created by the average operation. Therefore, it is reasonable to observe that 2-step ahead prediction is better than the one-step ahead case in Fig. 7.

m-GRU works similar to the function of PathAggregator in FlowNN, which also integrates the effect of congestion control in communications network. This explains the reason behind its superiority when comparing with other baselines in this tasks (but it also performs not good in the following cross-task learning test (Table 3) and model generality experiments (Table 4)). More details and intuition are provided in Appendix to interpret why the involved recurrent and graph convolutional operators in these baselines will fail to capture the data correlations manifested in the time-series tensor.

Transfer to end-to-end packet delay prediction task. It is important to guarantee that the provided end-to-end transmission delays meet users' agreement, such as a delay less than 50ms for online gaming. In real-world networks, many factors may influence the delay, including the dynamic traffic loads, packet congestion and queueing, etc. It is difficult to build an accurate delay model even for human experts (Xiao, He, and Gong 2018; Rusek et al. 2019). As explained

Table 3: Test performances of end-to-end packet transmission delay on unseen flows

	*	MSE	RSE	Corr
NUMFabric	1	0.1051±0.0046	0.3204±0.0046	0.9473±0.0012
	2	0.0386±0.0037	0.1942±0.0057	0.9811±0.0012
	3	0.0512±0.0036	0.2236±0.0053	0.9747±0.0013
	4	0.0346±0.0022	0.1841±0.0107	0.9831±0.0079
	5	0.0336±0.0032	0.1811±0.0057	0.9836±0.0011
WIDE	1	0.4002±0.0594	1.0371±0.0147	0.0355±0.0086
	2	0.3977±0.0768	1.0340±0.0675	0.3968±0.0292
	3	0.3877±0.0558	1.0209±0.0270	0.2013±0.0230
	4	0.4335±0.0609	1.0817±0.0406	0.2148±0.0058
	5	0.3168±0.0405	0.9228±0.0735	0.4571±0.0369

* : 1: GRU, 2: m-GRU, 3: STHGCN, 4: STGCN, 5: FlowNN

in **Congestion Control**, the dynamics of the past traffic and networking conditions will influence the choice of next-time sending rate and thus the transmission delay. This makes it possible to infer and predict the transmission delay from the behaviors of traffic sending rates.

In this task, we work on the same FlowNN model pretrained in next-step prediction task, and finetune a new MLP readout to predict the next-time-step transmission delay. Table 3 shows the test performances of different models. Although pretrained on the dataset of packet transmission rates, FlowNN still achieves the best results on the task of

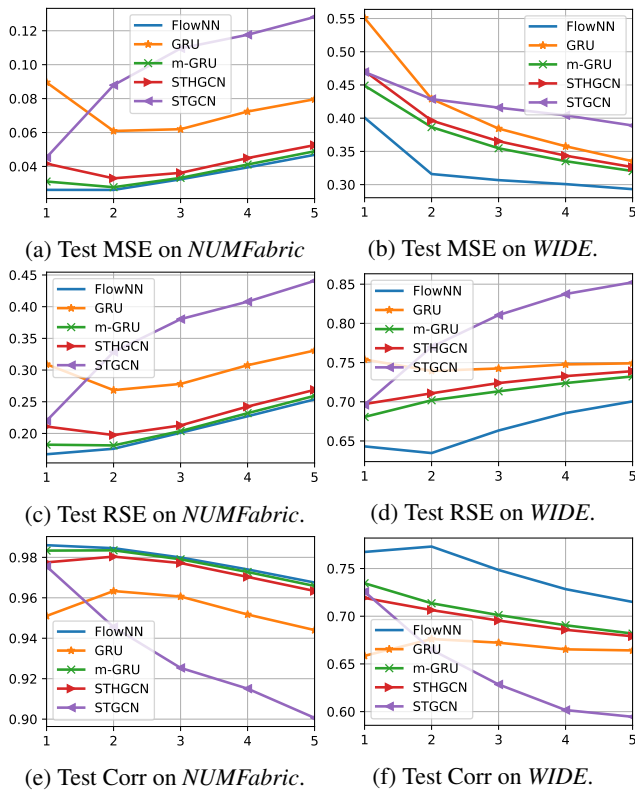


Figure 7: Prediction test performances on unseen flows under different steps ahead.

Table 4: Out-of-distribution test

*	MSE	RSE	Corr
1	0.5864±0.0123	0.7779±0.0085	0.6284±0.0108
2	0.5232±0.0111	0.7347±0.0076	0.6785±0.0085
3	0.5003±0.0107	0.7185±0.0083	0.6955±0.0088
4	0.4858±0.0050	0.7081±0.0033	0.7100±0.0035
5	0.3959±0.0078	0.6391±0.0084	0.7692±0.0072

* 1: GRU, 2: m-GRU, 3: STHGCN, 4: STGCN, 5: FlowNN

predicting a physical feature that is never included in the pre-training process. This shows the transferability of the self-supervised pretraining model of FlowNN across different learning tasks.

Generality test on Out-Of-Distribution dataset. We further test the model generality when a FlowNN model trained on one dataset, for example, *NUMFabric*, is used to work in an environment that is different from the trained one. Specifically, we froze the FlowNN model trained in next-step prediction task on the dataset *NUMFabric*, and finetuned a MLP readout to test its prediction performances on the dataset *WIDE*. To have a fair comparison, we also finetuned the readout layers of the frozen baselines trained on *NUMFabric* to test their performances on *WIDE*. From the results in Table 4, we can observe that FlowNN preserves its best performances. We conjecture the source of improvement is from the physics information being encoded properly

in our FlowNN design, which are followed for all kind of flows or networking environment. By contrast, m-GRU degrades remarkably and gets worse even than the two graph models. This shows the good generality and robustness of FlowNN, as well as the necessity of physics in a learning model.

Computation Efficiency. On the computing device of single Nvidia P40 24GB GPU, FlowNN takes about 0.3ms to predict for one step. Such speed is enough to support even every ms prediction task. Moreover, many networking tasks only require predicting the average of next multiple steps in practice, which further alleviates the requirement on computation speed when deploying FlowNN.

Related Work

Traditional analytical models. The past decades have seen numerous packet analysis models proposed to mathematically model the network dynamics (Gebali 2015). For example, extensive studies use the Poisson model to characterize the traffic by assuming the arrival pattern between two successive packets follows Poisson process. Considering the heavy tailed distribution and burstiness of the data-center traffic, recent work in (Benson, Akella, and Maltz 2010) models the packet arrival pattern as a log-normal process. To capture the temporal patterns and make predictions accordingly, ARIMA is exploited in (Ergenc and Ertan 2019) to model the time-series packet traffic. These analytical models are normally bonded to the specific formulation assumptions. More importantly, these statistical models work at coarse time scales of hours and assume relatively smoother traffic patterns. However, many tasks require the flow statistics at a timescale of subsecond, e.g., packet forwarding/queueing configurations and realtime networking control. Additionally, most flows last less than 1 minute, as reported in many practical traffic measurements in e.g. (Greenberg, Hamilton, and Jain 2009; Benson, Akella, and Maltz 2010; Benson et al. 2011). This implies that tasks requiring analysis models at finer-grained time scales are beyond the capability of these traditional models.

Neural network based learning models. With data-driven learning, the packet analysis can be done through a representation learning task that extracts the spatio-temporal patterns within the time-series packet data. In this field, extensive existing neural networks fit this task, including Convolutional Neural Net (CNN, (Mozo, Ordozgoiti, and GoÁmez-Canaval 2018)), Graph Neural Net (GNN, (Rusek et al. 2019)), Recurrent Neural Net (RNN) as well as their variants and combinations (e.g., STHGCN (Marcus et al. 2020), STGCN (Yu, Yin, and Zhu 2018), and (Xiao, He, and Gong 2018; Bernardez et al. 2021)). The customized designs to the data-specific properties make the success of these existing models in their dedicated domains, such as the convolutional operation to capture the spatially local correlations in CNN, and the aggregation operation to extract the adjacent link correlations in GNN, and so on. As a system with clear system structure and working mechanism, the communications network presents its own specific data

properties, which are difficult to capture for the incumbent models if without any modification. Moreover, these existing studies only target at a coarse-grained timescale above minutes or even hours. Models at a sub-second granularity, as *FlowNN* functions, require deeply combining the spatio-temporal data trends, as well as the system structural knowledge and working mechanism.

Conclusion

In this paper, we formulated the dynamic analysis problem of information flows in communication networks, and developed a customized neural network–FlowNN and the associated self-supervised training strategy to extract the domain-specific spatio-temporal data correlations within its time-series tensor. This study makes the pioneering work to design customized neural network and learning strategy by deeply combining the network structure and working mechanism. For this work, we also rely on the finetuning stage to adapt the pretrained model to the diverse downstream tasks or environment. Nevertheless, we want to highlight that the self-supervised learning strategies for our model is able to learn a physical bias that is universally transferable provided that the new network follows the same working mechanisms. This again explains the necessity to encode the physical knowledge into a neural network model. Because the patterns manifested by the data itself may vary in different environment, but the underlying physical working mechanism normally keeps invariant as long as the new environment follows the same working principle, e.g., TCP/IP. We reported the state-of-the-art performances for multiple practical networking application tasks, which demonstrates the strength of our approach. As a new ‘playground’ for both networking and deep learning communities, the research of network intelligence is still in its infancy. We hope this work will inspire more innovations in this field in the future.

Appendix A Sending Packets of Data with Congestion Control

In a communications network with Transmission Control Protocol/Internet Protocol (TCP/IP) suits, user’s messages are encapsulated into a set of small IP packets. Fig. 8–9 present the IP packet format and the sending process of IP packets.

Congestion control. When a TCP connection (or flow) is established between two end hosts, the sender will streams data packets to its receiver, and constantly receives the acknowledgement (ACK) as feedback about the sent packets from the receiver. When the data sending rate overwhelms the link bandwidth, congestion occurs and packets will be queued in buffers or dropped at congested nodes. Congestion increases the delay to receive the packet and thus degrades the overall transmission rates and delays.

With a congestion control model, the sender maintains a dynamic congestion window to limit the number of bytes that can be sent out in response to every ACK feedback.

For example, the CUBIC model (Ha, Rhee, and Xu 2016) uses the following growth function to determine the real-time congestion window $W(t)$:

$$W(t) = C(t - K)^3 + W_{max}, K = \sqrt[3]{\frac{W_{max}\beta}{C}} \quad (10)$$

where W_{max} is the window size after the last congestion event (i.e., packet loss/dropping is detected from ACK feedback); C and β are fixed constants; t is the elapsed time since the last window reduction.

Eq. 10 is adjusted every Round Trip Time (RTT) between the sender and receiver. Each RTT is normally a subsecond value. The quick adjustment avoids the consistent congestion, but also making the sending rate of a flow vary frequently. The cumulative loading volume (or sending rates) of packets in the history determines the probability of packet loss. Such connection makes it possible to approximate the sending rules of Eq. 10 from historical traces of sending rates of all flows. This explains the necessity of including the PathAggregator in FlowNN to approximate the decision process of the congestion control model.

Hop-by-hop data transmission. Once the allowed sending bytes/rates are determined by the congestion control model, the sender will encapsulate the data bytes into packets and send them out sequentially.

As an exemplary illustration in Fig. 9, let’s assume the network is configured with enough link bandwidth and initially there is no packet in the network. Assume $1MB$ of data are sent out from the sender node n_0 at the first time interval $t = 1ms$. By certain delay (e.g., $1ms$) due to link propagation and packet processing, the first $1MB$ of data will arrive at its next routing node R_1 at $t = 2ms$. In this case, at $t = 1ms$, the sending rates at the sender node n_0 and router R_1 are $x_{r,n_0}^{t_1} = 1Gbps$ and $x_{r,R_1}^{t_1} = 0Gbps$, respectively. At $t = 2ms$, the associated sending rates at R_1 becomes $x_{r,R_1}^{t_2} = 1Gbps$, while $x_{r,n_0}^{t_2}$ is again determined by the congestion control model according to the perceived historical information along the routing path. This forwarding process continues until reaching the destination (the receiver).

The above hop-by-hop data transmission establishes a special connection between the space and time. We can observe that $x_{r,R_1}^{t_2} = 1Gbps$ is physically determined by $x_{r,n_0}^{t_1} = 1Gbps$, the history information of its predecessor node (i.e, source n_0) rather than its own history information $x_{r,R_1}^{t_1} = 0Gbps$. Therefore, such time-resolved flow data not only tells us *who* is related to whom but also *when* and in which *order* relations occur. As analyzed in Appendix B, this provides the specific relational bias for the design of FlowNN.

Appendix B Relational Inductive Bias of Different Models

Many approaches in machine learning use a *relational inductive bias* (Peter et al. 2018) to impose constraints on relationships and interactions among entities in a learning process. Relational bias can be understood in terms of the bias-variance tradeoff (Geman, Bienenstock, and Doursat 1992),

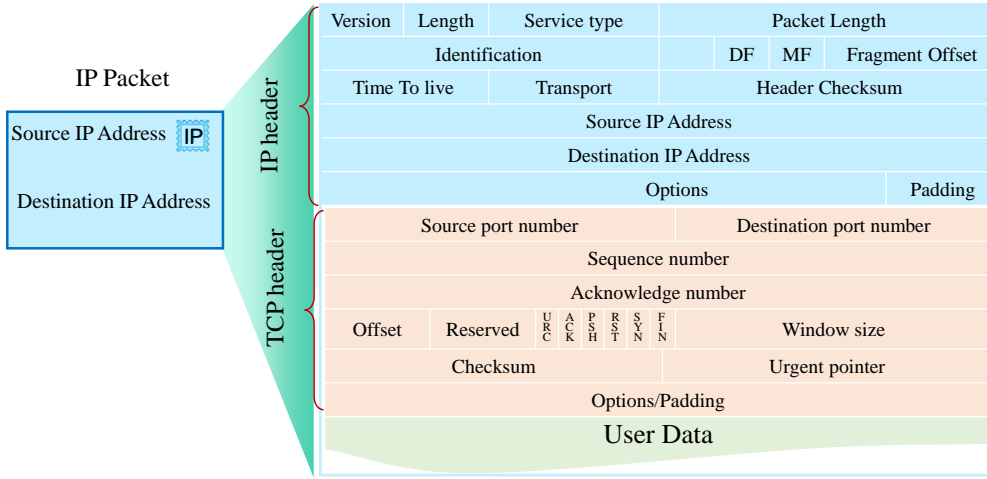


Figure 8: Encapsulation format of TCP/IP packet.

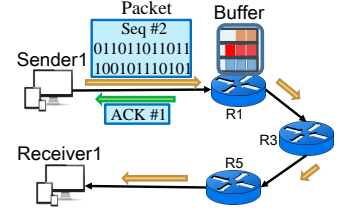


Figure 9: Data transmissions between two end hosts.

which help improve solutions that can generalize in a desirable way. However, mismatched relational bias will lead to suboptimal performance by introducing incorrect constraints. The elementary building blocks and their compositions involved in FlowNN and baselines also carry various relational inductive biases.

Recurrent and convolutional layers in baselines. The popular recurrent and/or convolutional layers are used in the compared baselines. For example, with a convolutional layer, STHGCN and STGCN actually are imposing locality as the inductive bias. Locality reflects that the arguments to the relational rule are those entities in close proximity with one another in the input signal’s coordinate space, *isolated* from distal entities (Peter et al. 2018). Similarly, the recurrent units in GRUs also carry a bias for temporal locality in the sequence. Therefore, with these build blocks, all these baselines are to predict with *all entities* in both spatially and temporally close proximity in the time-series tensor.

PathAggregator and Induction layers in FlowNN. With PathAggregator, FlowNN only relates (predicts) the states of source node \hat{h}_1^t with all historical information of $\{\hat{h}_n^\tau\}_{n=1, \dots, L, \tau < t}$. However, to predict states of spatial nodes $n = 2, \dots, L$, the Induction layer only relates the spatial information of \hat{h}_{n-1}^τ at its correlated time window. This filters out the irrelevant entities at the space-time coordinates that otherwise will be included as undesired noise.

Fig. 10 depicts the relational biases represented by different models. FlowNN attends to the physical inductive bias that matches the natural generating behaviors of the time-series tensor. On the contrary, all the baselines fail to match.

Appendix C Stop-Gradient for FlowNN

Following the analysis in (Chen and He 2021; Grill et al. 2020), let’s consider a loss function of the following form:

$$\mathcal{L}(\theta, \eta) = \mathbb{E}_X \left[\left\| \mathcal{F}^\theta(X) - \mathbb{E}_{\mathcal{T}} [f_{L_1}^\eta(\mathcal{T}(X))] \right\|_2^2 \right] \quad (11)$$

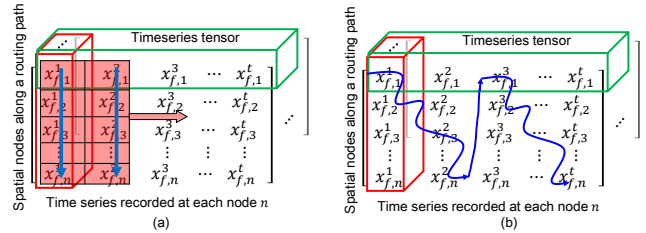


Figure 10: (a) Relational bias in baselines; (b) relational bias in FlowNN

where \mathcal{F}^θ is the compound neural net with parameter θ by encoder f_{L_1} and FlowNN g in Fig. 6; $\eta \subset \theta$ is the parameter to be learnt for f_{L_1} ; X is a sample of the input time-series tensor; \mathcal{T} is the augmentation operator.

Eq. 11 is equivalent to the cosine similarity loss if all vectors are l_2 -normalized. With this formulation, the training process updates the FlowNN at each step so that the learned FlowNN works for all possible input X . This is optimized by solving the following problem w.r.t θ and η :

$$\min_{\theta, \eta} \mathcal{L}(\theta, \eta) \quad (12)$$

The variable θ is learnt for the biased representation with FlowNN. The variable η is optimized for the representation of the input X with f_{L_1} . Formally, the problem in (12) can be solved by alternatively solving the following two sub-problems:

$$\theta^t \leftarrow \arg \min_{\theta} \mathcal{L}(\theta, \eta^{t-1}) \quad (13)$$

$$\eta^t \leftarrow \arg \min_{\eta} \mathcal{L}(\theta^t, \eta) \quad (14)$$

where t is the index of alternation and \leftarrow means assigning.

Subproblem (13) optimizes the learned physical bias from FlowNN under fixed encoder $f_{L_1}^{\eta^{t-1}}$. The *stop-gradient operation* in Fig. 6 is a natural implementation, since the gradient does not back-propagate to η^{t-1} (a constant) in this subproblem.

Table 5: Efficacy of different iterations N within FlowNN.

N	MSE	RSE	Corr
1	0.0274±0.0010	0.1711±0.0020	0.9853±0.0004
2	0.0261±0.0009	0.1672±0.0021	0.9860±0.0004
3	0.0273±0.0009	0.1710±0.0021	0.9854±0.0004
4	0.0286±0.0010	0.1747±0.0022	0.9849±0.0004
5	0.0280±0.0009	0.1731±0.0022	0.9849±0.0004

Likewise, the subproblem (14) can also be solved under fixed θ^t . By definition in Eq. 11, η^t is expected to minimize the average representations over any possible augmentation \mathcal{T} (i.e., any input X). Here, \mathcal{T} implies another view due to its random nature. In practice, it is unrealistic to actually compute the expectation $\mathbb{E}_{\mathcal{T}}$. Similar to (Chen and He 2021), we alternatively apply a neural network f_m (a MLP projection in the experiments) in Fig. 6 to predict the expectation. This reduces the subproblems into the following form:

$$\theta^{t+1} \leftarrow \arg \min_{\theta} \mathbb{E}_X \left[\left\| \mathcal{F}^{\theta}(X) - f_m(f_{L_1}^{\eta^t}(X)) \right\|_2^2 \right] \quad (15)$$

Here, parameter η is a subset of parameter θ . Therefore, problem (15) can be solved by one-step gradient update.

Appendix D Extra Experimental Results

Efficacy of different recurrent iterations N . Table 5 presents the test results on unseen flows of dataset *NUM-Fabric*. $N = 2$ achieves the best results, but other values of N do not degrade the performance remarkably. This shows that extra iterations can further improve FlowNN. Although FlowNN holds robustness across different N , improperly setting N will lead to very different computational complexity. Consequently, smaller N is more preferred.

Appendix E Reproducibility

Details of datasets. *NUMFabric* is a synthetic dataset collected by the NS-3 based simulator⁷ according to the configurations in (Nagaraj et al. 2016). The original simulator is configured with a 3-layer fat-tree network topology. While we used the same simulator by replacing the network topology as NSFNet topology and Germany 50 nodes topology from the site⁸ to generate the synthetic datasets of *NSF* and *GM50*, respectively. Instead of synthetic traffic patterns, dataset *WIDE* is collected with the realistic packet traces from site⁹.

For all datasets, we collected the real-time sending rates of 50 random flows, as well as the aggregated sending rates along the routing path at a time interval of 1ms with a total running length of 30000ms. The sending rates are calculated by counting the packets received/transmitted every ms from corresponding flows at each node. For the first 40 flows, we split the time length of 30000ms into training, validation and test by ratio 6:2:2. Therefore, only historical data were exposed during training. The evaluation and test processes

were both conducted with future data. Finally, we also tested the learnt model on the remaining 10 flows (unseen flows) that are never seen during training and evaluation.

Details of experiments. For all baselines, we conduct grid search over the hyper-parameters. The hidden size is chosen from {16, 32, 64, 128, 256} for all datasets. For all applied GRUs, the number of GRU layers is chosen from {1, 2, 3, 4}. For FlowNN, the iteration N is chosen from {1, 2, 3, 4, 5}. We used the library from site¹⁰ for the implementations of GCN in STHGCN. For STGCN, we followed the implementations released in site¹¹.

References

- Apice, C. D.; Manzo, R.; and Piccoli, B. 2008. A fluid dynamic model for telecommunication networks with sources and destinations. *SIAM J. Appl. Math.*, 68: 981–1003.
- Benson, T.; Akella, A.; and Maltz, D. A. 2010. Network traffic characteristics of data centers in the wild. *IMC*, 1–14.
- Benson, T.; Anand, A.; Akella, A.; and Zhang, M. 2011. MicroTE: fine grained traffic engineering for data centers. *IMACM CoNEXTC*, 1–12.
- Bernardez, G.; Suarez-Varela, J.; Lopez, A.; Wu, B.; Xiao, S.; Cheng, X.; Barlet-Ros, P.; and Cabellos-Aparicio, A. 2021. Is machine learning ready for traffic engineering optimization? *International Conference on Network Protocols (ICNP)*.
- Chen, X.; and He, K. 2021. Exploring simple siamese representation learning. *CVPR*.
- Chung, J.; Gulcehre, C.; Cho, K.; and Bengio, Y. 2014. Empirical Evaluation of Gated Recurrent Neural Networks on Sequence Modeling. *NIPS Deep Learning Workshop*.
- Ergenc, D.; and Ertan, O. 2019. On network traffic forecasting using autoregressive models. *arXiv preprint arXiv:1912.12220v1*.
- Gebali, F. 2015. *Modeling network traffic*, 445–492. Cham: Springer International Publishing. ISBN 978-3-319-15657-6.
- Geman, S.; Bienenstock, E.; and Doursat, R. 1992. Neural networks and the bias/variance dilemma. *Neural Computation*, 4(1): 1–58.
- Greenberg, A.; Hamilton, J. R.; and Jain, N. 2009. V12: a scalable and flexible data center network. *SIGCOMM*, 1–12.
- Grill, J.-B.; Strub, F.; Altche, F.; Tallec, C.; Richemond, P. H.; Buchatskaya, E.; Doersch, C.; Pires, B. A.; Guo, Z. D.; Azar, M. G.; Piot, B.; Kavukcuoglu, K.; Munos, R.; and Valko, M. 2020. Bootstrap your own latent: A new approach to self-supervised learning. *NeurIPS*.
- Ha, S.; Rhee, I.; and Xu, L. 2016. Cubic: a new TCP-friendly high-speed TCP variant. *SIGOPS-OSR*.

⁷<https://bitbucket.org/knagaraj/numfabric/src/master/>

⁸<http://www.knowledgedefinednetworking.org/>

⁹<https://mawi.wide.ad.jp/mawi/>

¹⁰<https://www.dgl.ai/>

¹¹<https://github.com/VeritasYin/STGCN.IJCAI-18>

Kipf, T. N.; and Welling, M. 2016. Semi-Supervised Classification with Graph Convolutional Networks. *NeurIPS*.

Lei, K.; Qin, M.; Bai, B.; Zhang, G.; and Yang, M. 2019. GCN-GAN: A Non-linear Temporal Link Prediction Model for Weighted Dynamic Networks. *IEEE INFOCOMM*.

Marcus, K.; Min, Z.; Chengzhi, Z.; Hanling, Y.; and Lujia, P. 2020. Spatio-Temporal Hybrid Graph Convolutional Network for Traffic Forecasting in Telecommunication Networks. *arXiv:2009.09849v1*.

Mozo, A.; Ordozgoiti, B.; and GoÁmez-Canaval, S. 2018. Forecasting short-term data center network traffic load with convolutional neural networks. *PLoS ONE*, 13(2): 1–31.

Nagaraj, K.; Bharadia, D.; Mao, H.; Chinchali, S.; Alizadeh, M.; and Katti, S. 2016. NUMFabric: Fast and Flexible Bandwidth Allocation in Datacenters. *ACM SIGCOMM*, 188–201.

Nathan, J.; Noga, H. R.; P.Brighten, G.; Michael, S.; and Aviv, T. 2019. A deep reinforcement learning perspective on internet congestion control. Proceedings of the 36th International Conference on Machine Learning.

Oord, A. v. d.; Li, Y.; and Vinyals, O. 2019. Representation Learning with Contrastive Predictive Coding. *arXiv preprint arXiv:1807.03748v2*.

Peter, W. B.; Jessica, B. H.; Victor, B.; Alvaro, S.; Viničius, Z.; and Mateusz, M. 2018. Relational inductive biases, deep learning, and graph networks. *arXiv preprint arXiv:1806.01261*.

Rusek, K.; Suarez-Varela, J.; Almasan, P.; Barlet-Ros, P.; and Cabellos-Aparicio, A. 2019. RouteNet: leveraging graph neural networks for network modeling and optimization in SDN. *arXiv preprint arXiv:1910.01508*, 1–12.

Sutskever, I.; Vinyals, O.; and Le, Q. V. 2014. Sequence to sequence learning with neural networks. *NeurIPS*, 3104–3112.

Wang, X.; Smith-Miles, K.; and Hyndman, R. J. 2006. Characteristic-Based Clustering for Time Series Data. *Data Mining and Knowledge Discovery*, 13(3): 335–364.

WIDE. 2020. <https://mawi.wide.ad.jp/mawi/>.

Xiao, S.; He, D.; and Gong, Z. 2018. Deep-q: Traffic-driven qos inference using deep generative network. *Proceedings of the 2018 Workshop on Network Meets AI & ML*, 67–73.

Yu, B.; Yin, H.; and Zhu, Z. 2018. Spatio-temporal graph convolutional networks: a deep learning framework for traffic forecasting. *IJCAI*.